FRET and Competing Processes between Conjugated Polymer and Dye Substituted DNA Strands: A Comparative Study of Probe Selection in DNA Detection

Hameed A. Al Attar* and Andy P. Monkman

Organic Electroactive Materials Research Group, Department of Physics, University of Durham, South Road, Durham DH1 3LE, United Kingdom

Received October 21, 2008; Revised Manuscript Received February 16, 2009

Fluorescence resonance energy transfer (FRET) between water-soluble conjugated polymer, poly-(9,9-bis(6′-*N*,*N*,*N*-trimethylammonium)-hexyl-fluorene phenylene) bromide, and ssDNA's labeled with four different types of dyes (Pacific-blue, Alexa-fluor 430, Fluorescein, and ROX) has been investigated. The effect of spectral overlap and Stokes-shift on the efficiency and properties of FRET were studied. In the DNA sequence detection technique that using cationic conductive polymer and the negatively charged DNA the electrostatic interaction leads to strong aggregation. The effective concentration of these aggregates is quite high leading to strong self-absorption. In this case, labeling with small Stokes shift dyes shows a strong output emission limitation even in extremely dilute system. The steady state fluorescence quenching of the CCP by FRET reveals that the competition between FRET and self-absorption plays a major role when accounting for the FRET ratio. Time-resolved fluorescence lifetime analysis was carried out to measure the energy transfer between the donor and the acceptor excluding self-absorption and quenching by ground-state complex formation. Time-resolved analysis indicates only around 30% of the total CCP excited-state population is quenched by FRET, whereas 55% is quenched by the DNA/buffer solution.

1. Introduction

Fluorescence resonance energy transfer-based sensors have recently been developed and have found uses in various applications. The most common application of FRET is to measure the distances between two sites comparable to the dimensions of biological macromolecules.[1] FRET sensors have also been developed for DNA and RNA hybridization studies.[2−4] Recent research in this area has focused on improving the donor and acceptor pairs to reduce false-positive signals.[5−7] A proper selection of the donor and acceptor is the key point for efficient resonance energy transfer and accurate measurement of the Förster radius. Melissa et al.[8] have experimentally determined the Förster distances R_0 of several donor−acceptor pairs, and they concluded that the observed difference in R_0 is largely due to changes in donor quantum yield. Various FRET-based strategies for nucleic acid detection have been used such as molecular beacons,[9] duplex probes,[10] scorpion primers,[11] and fluorescence polarization assays.[12] Several combinations of donor−acceptor pairs have been utilized, the donor fluorophore could be a single fluorophore such as a molecular dye or a nanoparticle (quantum dot donor) or multifluorophore system such as conjugated polymer. Conjugated polymer donors seem to have more promising potential characteristics to replace the conventional dye-based donor due to light harvesting and also possibly better control of the donor−acceptor separation for optimum FRET.[13] Conjugated polymers can also be synthesized in water-soluble form to be used in water-based biological assays.[14] Biological analyte detection using conjugated polymers has been suggested by Swager and co-workers and Whitten and co-workers[15,16] and various conjugated polymer/analyte detection methods have been demonstrated. Bazan and co-workers[17] suggested a method of DNA detection based on optical amplification of a probe signal by light harvesting from the water-soluble conjugated polymer. Recently we were able to detect a single nucleotide polymorphisim (SNP) that related to the *BCR-ABL* incogene (T315I) with a signal discrimination approach 75%[18] using water-soluble conjugated polymer as a donor and nonionic surfactant to enhance the sensitivity and the selectivity of the detection. Due to the multichromophor characteristics of the conjugated polymer and the efficient energy transfer by light harvesting, the acceptor should possess a good spectral overlap, which is paramount to high transfer efficiency. The donor and acceptor photoluminescence (PL) signals must also be well-resolved to extract accurate experimental information for the system under investigation. The quenching of the donor (CCP) by the acceptor (label DNA) may not be restricted to only the FRET process. The electrostatic and hydrophobic interactions between the positively charged CCP and negatively charged DNA may lead to contact quenching by the formation of a nonradiative ground-state complex (CCP/DNA) and photoinduced charge transfer (PCT) from the excited CCP to the DNA bases (specially with the lowest oxidation potential quinine dG[19]). The ground-state complex formation is a weak electrostatic complex, which does not show a change in the absorption signature of the donor. The quenching by this complexation arises predominantly from CCP aggregation by the DNA causing CCP−CCP interchain quenching.[20]

The FRET process is normally described by the dipole−dipole interaction and the rate of energy transfer is described by the Förster equation. Recently, it has been shown that two effects may violate Förster's rules: first, the interaction between the donor CCP and the acceptor by PCT, which depends on the relative HOMO and LUMO of the donor and acceptor;[21] second, the conformation effect due to the chemical structures of the donor and acceptor is a factor that may also violate Förster's

* To whom correspondence should be addressed. E-mail: h.a.al-attar@durham.ac.uk.

10.1021/bm801194n CCC: $40.75
Published on Web 04/01/2009

Table 1. Absorption, λ_{abs} max, Emission, λ_{em} max, Wavelength Maxima, Stokes Shift, Absorption Line Width, Δ_{abs}, Fluorescence Quantum Yields, Φ_{PL}, Fluorescence Lifetime, τ, Overlap Integral, $J(\lambda)$, and Förster Radii R_0 of the Four Dyes Used in DNA Labeling as Acceptors Together with the Cationic Conjugated Polymer CCP Donor Parameters Used in this Work

dye	λ_{abs} max (λ_{em} max) (nm)	Stokes shift (nm)	Δ_{abs} (nm)	Φ_{PL}	τ (ns)	$J(\lambda)$ 10^{14} (M^{-1} cm^{-1} $(nm)^4$)	R_0 (Å)
fluorescein	496 (520)	24	35	0.91	2.95	8.08	38.8
ROX	586 (604)	18	35	0.7	4.36	1.45	29.2
alexa-fluor	435 (536)	99	90	0.66	3.27	4.42	35.1
pacific-blue	404 (468)	54	50	0.78	2.86	3.7	34.1
CCP	380 (424)	44		0.34	0.5		

[a] The quantum yield of the dyes has been taken from the refs 32−35, respectively, and for the CCP in water has been measured.

rules due to enhanced acceptor stacking and the orbital interaction with the donor backbone.[22] Furthermore, theoretical work by Wong et al.[23] has shown that the conventional Förster theory does not hold in conjugated polymer system because of the effect of the dependence of the excitation rates on the distance and orientation of the conjugated polymer to the acceptor, that is, breakdown of the point dipole approximation.

In this work we have investigated the efficiency of FRET between a water-soluble conjugated polymer as a donor and four dye labeled ssDNA, which have different donor−acceptor spectral overlap functions and acceptors Stokes shift. The CCP and ssDNA-C* aggregation and their effects on the probe emission intensity as a function of the acceptor Stoke's shift are discussed. Absorption line widths of the acceptor may also play some rule to control the FRET efficiency. Steady state and time resolve fluorescence analysis were performed, and the rate of the energy transfer was determined.

2. Experimental Section

I. Materials and Methods. The CCP used was the cationic water-soluble conjugated polymer poly-(9,9-bis(6′-*N*,*N*,*N*-trimethylammonium)-hexyl-fluorene phenylene) bromide, **1**, molecular weight around 22000 g/mol, yielding 35 monomer units (fluorine-phenylene) per polymer chain.[24] The absorption and emission peaks of the CCP are at 380 and 424 nm, respectively. A 14-base ssDNA-C*, where C* is the dye attached at the 5′ (C*-5′-OO-ATG-TCA-ATG-AT-3′), were obtained from MWG Biotech. Four dyes were tested: fluorescein, Pacific-blue (3-carboxy-6,8-difluoro-7-hydroxycoumarin), Alexa-fluor 430, and ROX (carboxy-X-rhodamine). Some of the photophysical properties of these dyes are given in Table 1. The chemical structure of the water-soluble conjugated polymer and the ssDNA-C* used in this experiment are shown in Scheme 1. The absorbance of the labeled ssDNA was measured using Perkin-Elmer Lambda 19 spectrophotometer and the photoluminescence was measured using a Jobin Yvon Fluorolog spectrophotometer.

Time-resolved fluorescence decays were collected using picosecond time-correlated single photon counting (TCSPC) technique (IRF = 23 ps). The excitation source is a picosecond Ti:sapphire laser (MIRA) from Coherent Inc. (vertical polarization, wavelength range: 720−1000 nm, 76 MHz repetition rate) coupled to a second harmonic generator (360−500 nm). Emission collected at the polarization magic angle is detected through a double subtractive monochromator by a microchannel plate (MCPT) Hamamatsu model R3809U-50. Signal acquisition was performed using a TCSPC module (Becker & Hickl Model SPC-630). Deconvolution of the fluorescence decays was performed using Globals WE software package.[25]

II. DNA Quantification and Samples Preparation. To better visualize the effect of various label dyes on energy transfer by FRET from the donor (CCP) to the acceptor (dye) two restrictions should be considered. First, the quenching of the donor by ssDNA through CCP/ssDNA complexation and photoinduced charge transfer (PCT) between CCP and DNA should be the same for all types of dyes; this can be achieved by using a same DNA basis number and sequence and quantifying the DNA concentration by measuring the absorbance at 260 nm. Because the ssDNA base sequence does not change for different DNA-C* labeled dyes, therefore, the absorbance at 260 nm is directly proportional to the concentration of the DNA in the assay, which can be adjusted to be the same. We should note here that any absorbance of the dye at 260 nm is accounted for; Figure 1 shows the quantification of DNA after correction for the dyes absorbance at 260 nm, showing about the same DNA absorbance at 260 nm.

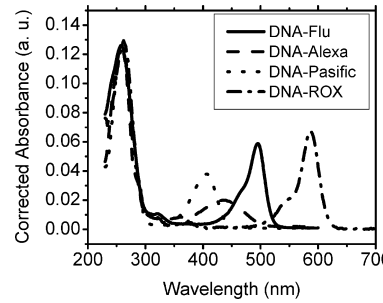

Figure 1. Absorbance spectra of each ssDNA-C* used in this work. The absorbance at 260 nm were corrected to quantify the same amount of DNA and to compare the absorbance spectra of the quenchers. The concentrations for all ssDNA-C* were 4×10^{-7} M.

Scheme 1. Chemical Structure of Water-Soluble Polyfluorene Poly-(9,9-bis(6′-*N*,*N*,*N*-trimethylammonium)-hexyl-fluorene phenylene) Bromide (CCP) **1**. ssDNA Labeled with Different Dyes: Pacific Blue (PB) **2**, Fluorescein (FL) **3**, Alexa-fluor 430 (AF) **4**, and ROX (R) **5**

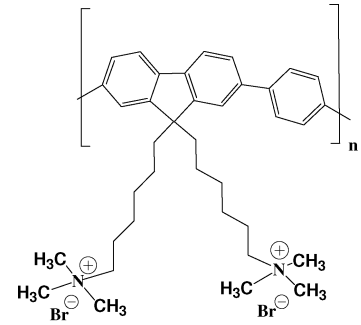

1

Second, due to the possibility of contamination by unlabeled DNA, the labeling efficiency, which is defined as the concentration ratio of the dye to the DNA ([dye]/[oligo]) should be around 1.0 (approximately one dye molecule per DNA molecule). The labeling efficiency η can be estimated using the formula[26] $\eta = (\varepsilon_{260}/\varepsilon_{dye})/(A_{260}/A_{dye})$, where, ε_{260} is the extinction coefficient at 260 nm of an oligonucleotide and can be estimated from the nucleotide composition as the sum of the extinction coefficients of the individual nucleotides (dATP = 15.4 mL μmol^{-1} cm^{-1}, dCTP = 7.3 mL μmol^{-1} cm^{-1}, dGTP = 11.7 mL μmol^{-1} cm^{-1}, and dTTP = 8.8 mL μmol^{-1} cm^{-1}). For the present 14 nucleotides DNAs (5′-ATG AAC TCA ATG AT-3′), the calculated extinction coefficients are ε_{260} = 165.6 mL μmol^{-1} cm^{-1}. The extinction coefficients of the label dyes were taken from MWG Biotech company,[27] which are fluorescein = 83 mL μmol^{-1} cm^{-1}, Pacific blue = 37 mL μmol^{-1} cm^{-1}, Alexa-fluor 430 = 16 mL μmol^{-1} cm^{-1}, and ROX = 82 mL μmol^{-1} cm^{-1}. The estimated efficiency using the above η formula was 0.95, 1.05, 1.18, and 1.04 for the dyes, respectively. Considering inaccuracies in the estimation of the extinction coefficients of oligonucleotides, these values indicate about 1:1 dye to oligo molecules and negligible free dyes in the solution.

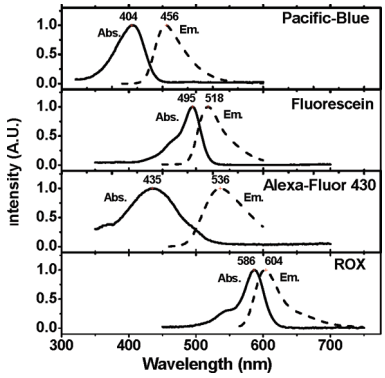

Figure 2. Normalized absorbance and photoluminescence (PL) spectra of the donor the acceptor dyes Pacific blue (PB) **2**, fluorescein (FL) **3**, Alexa-fluor 430 (AF) **4**, and Rox (R) **5** in 10 mM phosphate buffer (pH = 7.4).

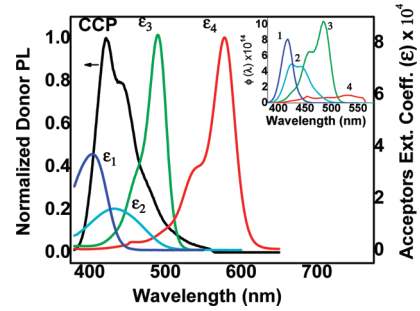

Figure 3. Normalized fluorescence emission of the donor (CCP) (left scale) and the absolute value of the acceptor (dyes) extinction coefficients ε_i (right scale), where $i = 1$ (Pacific blue), **2** (Alexa-fluor 430), **3** (fluorescein), and **4** (ROX). Inset is the overlap parameter $\varphi(\lambda)$, where the overlap integral is given by $J(\lambda) = \int \varphi(\lambda)\, d\lambda$.

3. Results and Discussion

I. Steady State Photophysical Analysis. The dyes were selected so that they give different spectral overlap, Stoke's shift and absorption line width. The emission of the donor CCP **1** peaks at 424 nm. The peak emissions of the dyes in aqueous 10 mM phosphate buffer (pH = 7.4) are 456 nm for the Pacific blue (PB) **2**, 518 nm for the fluorescein (FL) **3**, 536 nm for the Alexa-fluor 430 (AF) **4**, and 604 nm for the ROX (R) **5**. Figure 2 shows the normalized absorption and emission of the four dyes. The Stoke's shift, the absorption line broadening, and the quantum yields of the four dyes are given in Table 1.

In the point-dipole approximation model, the fluorescence resonance energy transfer (FRET) rate (K_{FRET}) from a donor to an acceptor positioned at a distance r_{DA} is described by the long-range excitation energy transfer from the donor to acceptor via the dipole−dipole interaction, which is described by Förster[28,29]

$$\kappa_{FRET} = \frac{1}{\tau_D}\left(\frac{R_0}{r_{DA}}\right)^6 \tag{1}$$

where

$$R_0 = \left[\frac{9000(\ln 10)Q_D\kappa^2 J(\lambda)}{128\pi^5 N n^4}\right]^{1/6} \tag{2}$$

$$J(\lambda) = \frac{\int_0^\infty F_D(\lambda)\varepsilon_A(\lambda)\lambda^4 d\lambda}{\int_0^\infty F_D(\lambda) d\lambda} \tag{3}$$

where τ_D is the lifetime of donor in the absence of acceptor, Q_D is the quantum yields of the donor in the absence of acceptor, N is Avogadro's number, n is the refractive index of the medium, and κ^2 is a factor describing the relative orientation of the transition dipoles of the donors and acceptor. The integral, $J(\lambda)$, expresses the degree of spectral overlap between the emission of the donor, $F_D(\lambda)$, and the absorption of the acceptor, $\varepsilon_A(\lambda)$. R_0 is called the Förster distance. The point-dipole approximation used to derive the Förster formula above is not accurate in the case of the conjugated polymer, as these donors have extended dipole moment densities that are spread along the donor (polymer chain). It has been shown[30] that the conventional Förster expression overestimates the energy transfer rate by more than 2 orders of magnitude at short separation ($R_{DA} < 1$ nm). In a dilute solution (ssDNA and CCP concentrations $\approx 10^{-7}$ M) and with the conjugated polymer side groups larger than 1 nm in length, as in our case, the conventional Förster theory may still be used. We have also seen that at short donor acceptor distances <1 nm the quenching by charge transfer is far greater than the energy transfer by FRET. However, the quenching mechanism at donor−acceptor distances smaller than 1 nm is quite complicated and is not well understood. The absolute value of the calculated energy transfer rate may be slightly different from the real value at distances greater than 1 nm, but the relative value for each dye acceptor in our experiment will be the same because only one type of water-soluble conjugated polymer "donor" has been used in this experiment. Figure 3 shows the normalized fluorescence emission of the donor (CCP; left scale) and the absolute value of the acceptor (dyes) extinction coefficients ε_i (right scale), where $i = 1$ (Pacific blue), **2** (Alexa-fluor 430), **3** (fluorescein), and **4** (ROX). The overlap parameter as a function of wavelength $\varphi(\lambda)$ is plotted, where the overlap integral is the area under the curve, which is given by $J(\lambda) = \int \varphi(\lambda)\, d\lambda$, and the values of the $J(\lambda)$ for the four dyes are given in Table 1. The calculated Förster radii using the expression $R_0 = 0.211 \times (n - 4\kappa^2 Q_D J(\lambda))^{1/6}$ in Å,[29] indicates that the FL dye has the maximum overlap spectral function as shown in Figure 3 and Table 1. Because all DNA-C* have the same oligonuclutide sequence and density of charge, r_{DA} (the actual donor−acceptor distance) should be the same for all CCP/DNA-C* complexes. Therefore, we expect that the higher Förster radii should give higher energy transfer.

In CCP/DNA-C* systems the quenching by FRET, PCT, complexs formation, and so on is also donor concentration dependent (this is due to the acceptor aggregation by CCP, see below). Therefore, it is necessary to ensure that the initial donor concentration used in each quenching experiment for different acceptor types are approximately the same. Figure 4 shows the fluorescence spectra of the CCP-DNA-C* mixture as a function of ssDNA-C* concentration. The initial addition of DNA-C* 2×10^{-8} M to the CCP solution causes the CCP fluorescence to be quenched strongly by about 80−90% of its original value for all the different ssDNA-C*. This quenching is due to FRET and non-FRET processes (i.e., contact quenching, self-quenching by aggregation, etc.). The non-FRET quenching is approximately the same because it is not strongly dependent on the spectral overlap. By comparing the amount of donor quenching and acceptor emission signals in Figure 4, we concluded that quenching by complexation and PCT reduces the donor efficiency by more than 70%. This result also indicates that the initial amount of the negatively charged DNA added is strongly attracted to the CCP, forming electrostatic complexation, and

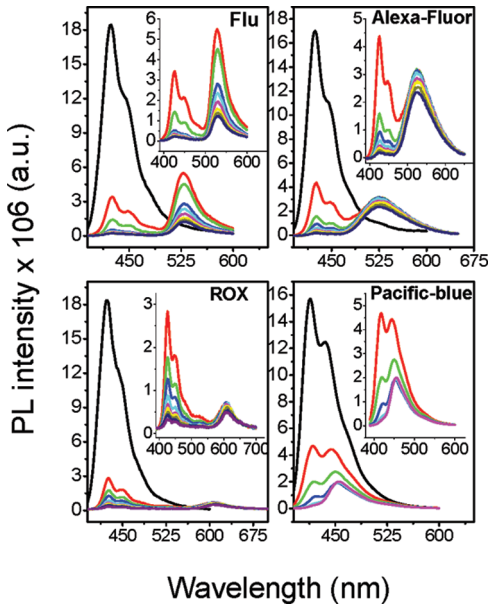

Figure 4. Fluorescence spectra of the donor CCP (1×10^{-6} M) at various acceptor ssDNA-C* concentrations ($0-1.6 \times 10^{-7}$ M) in 10 mM phosphate buffer. Inset 1 shows the same figure without the initial unquenched CCP signal (black lines without acceptor). Excitation wavelength = 380 nm.

causes the CCP to quench mainly by nonradiative contact processes or CCP−CCP interaction. In our previous DNA detection studies[31] we proved that by using nonionic surfactants, for example, the contact quenching can be reduced by forming aggregate or binary micelles between the surfactant and the CCP, which slightly separates the CCP/DNA from each other, suppresses the short-range charge transfer contribution, and enhances the external energy transfer by FRET. However, the amount of surfactant required to achieve such enhancement is very critical because the increase in the distance between the donor and the acceptor will also reduce FRET due to the efficiency of FRET being inversely proportional to the power six of the donor acceptor distance. Analyzing Figure 4 we see that only DNA labeled with fluorescein and Alexa-fluor give a well-resolved and sufficient acceptor signal, while the Pacific blue FRET signal is not well-resolved from the unquenched CCP emission and the ROX signal is highly resolved but very weak. Figure 4 shows that Alexa-fluor appears to be a better acceptor than fluorescein, which contradicts the Förster equation given the relative strengths of the spectral overlap of the two dyes, as shown in Figure 3 and Table 1.

To study the quenching mechanism and FRET ratio, a modified Stern-Volmer relation, as given by $PL_0/PL = 1 + K_S[DNA]$, and the FRET ratio defined as the ratio of the integrated PL intensity of the acceptor to the integrated PL intensity of the donor, given by $\int PL_{acceptor}/\int PL_{donor}$, were investigated. Where PL_0 is the intensity of fluorescence in the absence of the quencher (DNA-C*) and PL is the intensity of fluorescence in the presence of the DNA-C* and $\int PL_{acceptor}$ is the integrated acceptor emission spectrum and $\int PL_{donor}$ is the integrated donor emission spectrum. In all cases, the raw PL spectra were corrected to account for the direct excitation of the acceptor and also for spectral overlap of the donor emission to calculate deconvoluted spectra in order to obtain separate signals characteristic of the different fluorophores. Two different excitation wavelengths were used, 340 and 380 nm. For 340 nm excitation, the direct excitation for all fluorophores is negligible, but the spectra were relatively weak. For the

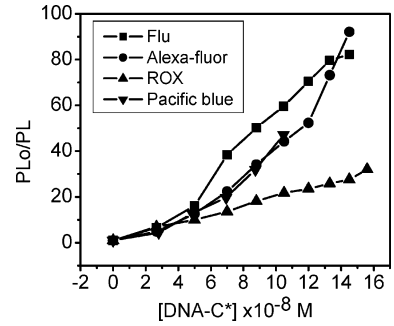

Figure 5. Stern-Volmer plot showing the quenching efficiency of the CCP (1×10^{-6} M) at various DNA-C* concentration. Fluorescence data obtained from integral spectra in figure 4. Excitation wavelength = 380 nm.

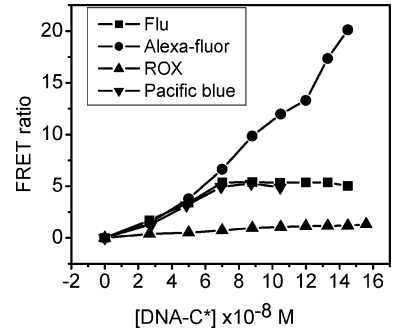

Figure 6. FRET ratio of different ssDNA-C* acceptors at various concentration $0-1.6 \times 10^{-7}$ M with a donor CCP concentration of 1×10^{-6} M. Excitation wavelength = 380 nm.

excitation at 380 nm (peak donor absorption), all signals are strong with appreciable acceptor PL signal due to direct excitation being measured, especially for the ROX fluorophore, which has relatively higher absorption at this wavelength. In all cases, the direct excitation signal at different acceptor concentration is subtracted from the raw spectra to obtain the actual signal generated by FRET.

Deconvolution of the composite signal was performed by assuming a linear superposition of PL signals with known shapes, yielding individual spectra for the CCP and fluorophore for each quencher concentration. The quenching strength obtained from the Stern-Volmer relationship and the FRET ratio plots are depicted in Figures 5 and 6. However, a high quantity of donor excitons is quenched by non-FRET process (static and PCT). Figure 5 shows that for all ssDNA-C* systems an initial efficient donor exciton quenching by non-FRET process. Figure 5 also indicates that the donor quenching rate is proportional to the overlap function $J(\lambda)$, that is, larger $J(\lambda)$ shows higher quenching.

The FRET ratio as a function of DNA-C* concentration is plotted in Figure 6.The initial FRET ratio at [DNA-C*] $< 5 \times 10^{-8}$ M is also slightly higher for the C* = fluorescein. At [DNA-C*] $> 5 \times 10^{-8}$ M, the FRET ratio for all dyes tend to saturate, except for Alexa-fluor 430, which continues to increase above this acceptor concentration, giving a higher contrast value. The FRET ratio saturation correlates to the acceptor's Stoke shift and absorption line width (see Figure 2). However, it is surprising that an inner filter or self-absorption effect is effective in a solution of concentration $10^{-8}-10^{-7}$ M.

The negligible self-quenching by reabsorption in the acceptor only fluorescence experiment becomes effective due to both FRET and self-quenching by reabsorption rates are comparable in strength and compete against each other. In our previous

Scheme 2. Aggregation of the Negatively Charged ssDNA-C* around the Cationic Conjugated Polymer (CCP) Increases the Effective Concentration of the Dye (C*) and Induces Strong Self Reabsorption[a]

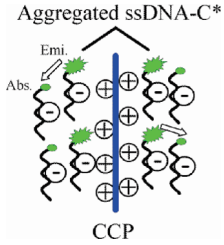

[a] Higher self reabsorption occurs in smaller Stoke's shift dye.

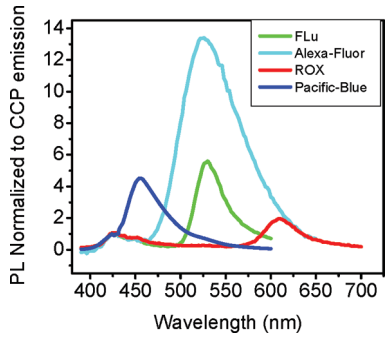

Figure 7. Emission spectra of the CCP/DNA-C* assays, where the donor CCP emission at 420 nm is normalized for each assay. CCP concentration was 1×10^{-6} M, the DNA-C* concentration was selected for maximum FRET ratio. Excitation wavelength = 380 nm.

work[31] we have shown in both steady state and time-resolved fluorescence measurements that the dye emission of the hybridized ssDNA/PNA-C* quenched when the donor CCP concentration increases and this is ascribed to the acceptor aggregation around the CCP. The aggregation between the negatively charged ssDNA-C* and the positively charged CCP increase the effective concentration of the acceptors and allows for efficient reabsorption, Scheme 2. It should be noted that ssDNA-C*/ssDNA-C* aggregation may also cause acceptor quenching by intermolecular interaction C*−C*.[31]

Figure 7 shows the PL emission of the CCP/ssDNA-C* at maximum energy transfer condition where the graphs are normalized to the donor emission at 424 nm. Setting the output window of the acceptor signal above 500 nm the number of photons provided by Alexa-fluor 430 is four times that provided by fluorescein.

II. Time-Resolved Analysis. In the steady state fluorescence measurements we noted that potentially the nonradiative ground-state electrostatic complex formed by the CCP and DNA-C* may substantially contribute to the total quenching mechanism. Self -quenching by reabsorption may also limit the output signal, especially in dyes with small Stokes shift. Time-resolved analysis provides an accurate measurement of the amount of energy transfer by FRET, excluding both ground-state quenching by complex formation and the inner filter effects. Time-resolved analysis of the CCP donor quenching by different acceptors DNA-C* at various concentration was therefore performed. Figure 8 shows an example of the time -resolved fluorescence decay of the CCP/DNA-Fluorescein system. The decay at 420 nm is for the CCP "donor" emission (a) and the decay at 520 nm is for the fluorescein acceptor emission (b) at various DNA-C* concentrations, the excitation wavelength was at 375 nm. Looking for the donor emission decay at various acceptor concentrations we identify two regions. The region below 0.25

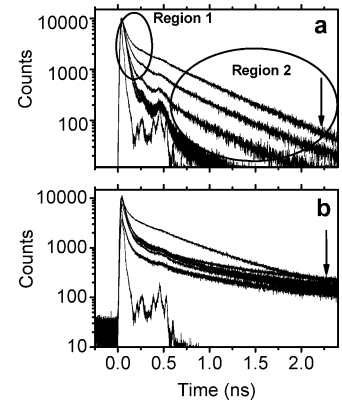

Figure 8. Time-resolved fluorescence decay of CCP/DNA-fluorescein system. The decay at 420 nm is for the CCP "donor" emission (a), and the decay at 520 nm is for the fluorescein acceptor emission (b) at various DNA-C* concentrations ($0-1.6 \times 10^{-7}$ M). The arrows indicate the increase of the DNA-C* concentration. Excitation wavelength = 375 nm.

ns which shows a change in the slope at different acceptor concentration and is assigned to the increase in the energy transfer as well as increases the interchain interactions (CCP−CCP aggregation by DNA[20] as a function of acceptor concentration). The second region lying above 0.5 ns shows decay independent of acceptor concentration (same slopes at various acceptor concentrations) and is assigned to the lifetime of the noninteracting, isolated polymer chains. The decay profile at the acceptor peak emission is quite complicated due to the inclusion of different decay processes such as the decay of an aggregated CCP (red-shifted excimer emission) as well as the decay of the growing acceptor signal. The decay profile at the acceptor emission may also contain the acceptor decay due to the presence of the donor. Similar sets of donor and acceptor decay profiles, as shown in Figure 8 for the different ssDNA-C*, were also obtained. To analyze the change in the different decay components as a function of acceptor concentration, a global analysis of the fluorescence decay of the donor at 424 nm (Figure 8a) and the acceptor at 520 nm (Figure 8b) data sets are fitted simultaneously with four discrete lifetimes using $I(t) = \sum_{i=1}^{j} a_i \exp(-t/\tau_i)$ and the four lifetimes are "linked" across the data sets. In this analysis, the lifetimes of the two sets stay the same, and only their fractional contributions are changed in the donor and acceptor emission spectra. The four decay components can be related to the three types of donor polymer chain stacking in solution; as we have previously identified,[20] these are isolated polymer chains with predicted lifetime $\tau \approx 500$ ps (i); loose clusters $\tau \approx 100$ ps (ii); aggregates $\tau \approx 20$ ps (iii); and the decay lifetime of the acceptor emission $\tau \approx 2-3$ ns (iv).

Due to limited energy transfer in the CCP/DNA-ROX system (very low overlap function) and low resolution in the CCP/DNA-Pacific blue system (donor emission at 424 nm and acceptor emission at 455 nm), only CCP/DNA-Flu and CCP/DNA-Alexa-fluor 430 systems have been considered in the following discussion. Figure 9 shows the fractional contribution of each component to the steady state intensity f_i, defined as[28] $f_i = a_i\tau_i/\sum_j a_j\tau_j$, for the emission at 424 and 520 nm, respectively. Inspecting Figure 9, we see that the contribution of the isolated polymer chain (i) decreases rapidly as DNA-C* concentration increases. The isolated polymer chain is the main fluorescence emission and the most efficient component that contributes to the total donor emission. This component is strongly quenched upon addition of the DNA-C*. The CCP quenching matches

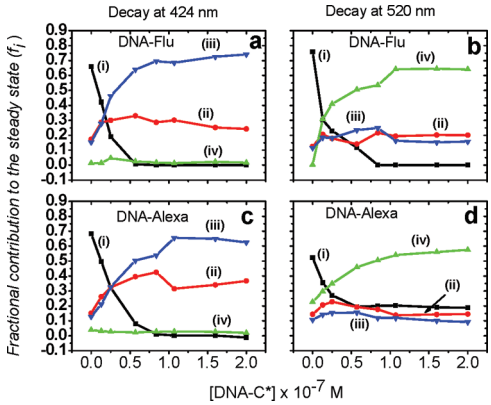

Figure 9. Fractional contribution of each decay component to the steady state intensity f_i, for the emission at 424 and 520 nm. The four decay components are (i) isolated polymer chain, (ii) aggregated polymer chain, (iii) clusters, and (iv) the decay component at the acceptor peak emission. Excitation wavelength = 374 nm.

well with the increase in FRET transferred to the acceptor emission as shown in (iv) at 520 nm. The CCP emission is further quenched by the DNA (photoinduced charge transfer) and by CCP−CCP aggregation, which give rise to the components (ii) and (iii). Because the DNA-C* concentration is the same for different dyes, the quenching strength of the isolated polymer chain at 424 nm (i) and the signal growth of the acceptor signal by FRET at 520 or 530 nm (iv) can be used to estimate the efficiency of the energy transfer between the donor and the acceptor. Figure 9 shows that the quenching of the donor and the growth of the fluorescein emission occurs at a higher rate than that for Alexa-fluor 430 at the initial low ssDNA-C* concentrations. This reflects the higher overlapping integral $J(\lambda)$ value of the fluorescein compared with Alexa-fluor 430. It should be noted that due to the unavoidable correlations between various emissive components, Figure 9 shows only the qualitative behaviors of these components.

To better visualize the energy transfer efficiency E_{DA}, we apply the relation $E_{DA} = 1 - (\langle\tau_{DA}\rangle/\langle\tau_D\rangle)$, where τ_D is the donor lifetime in the absence of the acceptor and τ_{DA} is the donor lifetime in the presence of the acceptor. The energy transfer efficiency is calculated for each acceptor concentration using the average lifetime $\langle\tau\rangle = \sum a_i\tau_i^2/\sum a_i\tau_i$, where i run over the decay components (i) and (ii) of the donor peak emission at 424 nm only. Components (iii) and (iv) are not included because in the time averaging component (iii) has negligible contribution to the energy transfer efficiency (i.e., predominantly interchain quenching) and component (iv) is related to the acceptor emission where the time decay increases with increasing acceptor concentration (i.e the acceptor emission decay time at 3 ns is dominant the decay process). The energy transfer efficiency versus DNA-C* concentration is shown in Figure 10. We were unable to measure the energy transfer efficiency of the DNA-Pacific blue due to strong donor−acceptor emission wavelength overlap.

Figure 10 shows that at low acceptor concentration (in general [DNA-C*] < [CCP]) the FRET efficiency is proportional to the overlap integral function. A higher overlap function gives a higher energy transfer rate, which is in agreement with Förster theory (this is also observed in the steady state measurements at initial low acceptor concentrations Figure 4). At specific acceptor concentrations, depending on the dye type and CCP concentrations, the FRET efficiency saturates at approximately 85%; no more energy transfer can be achieved. The quenching efficiency by nonlabeled DNA is also shown in Figure 10. This

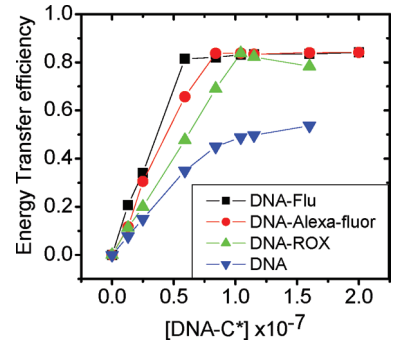

Figure 10. Energy transfer efficiency as a function of acceptor concentration. CCP concentration was 1×10^{-6} M. Blue triangles show quenching efficiency of nonlabeled DNA. Excitation wavelength = 374 nm.

non-FRET quenching is predominantly due to CCP−CCP aggregation by DNA (interchain interaction) and also possibly by photoinduced charge transfer. It should be noted that CCP quenching by the phosphate buffer has also been observed. Figure 10 shows that the CCP quenching by the DNA/buffer solution approaches 55% of the total CCP excited-state population. The saturation at 85% indicates that the CCP population quenched by the FRET process is around 30% while 15% of the total unquenched. This analysis indicates the importance of reducing the donor quenching by DNA/buffer and CCP aggregation. We have already employed a successful method using nonionic surfactant to reduce both CCP aggregation and quenching by DNA/buffer.[31]

4. Conclusion

In DNA sequence detection, the label dye that possesses larger Stokes shift provides better sensitivity. This is because even in very dilute CCP/ssDNA-C* assays the electrostatic attraction brings the constituents in close proximity, leading to aggregation in all systems. Therefore, the effective concentration of CCPs and acceptors is much higher in these aggregates. In this case the self-absorption will be high in small Stokes shift acceptors. We have proved that Alexa-fluor 430 can provide a better detection signal despite its low extinction coefficient. With the recent interest in using conjugated polymers as a donor to enhance the bioimaging technique in condensed media where the dye concentration is at high concentration, the Alexa-fluor 430 can be considered as an efficient acceptor conjugate. Time-resolved analysis is the most accurate method to quantify FRET efficiency due to the exclusion of the static quenching and self-quenching by reabsorption. From time-dependent measurements we have obtained that only 30% of the total donor excited-state population is transfer by FRET process. There is a large amount of donor energy dissipated by non-FRET quenching, which needs to be minimized to enhance the sensitivity of this method of detection.

Acknowledgment. The authors thank Dr. Mallavia and Marin Ricardo for the kind gift of the cationic conjugated polymer. This work has been financially supported by CENAMPS via the Durham University Photonic Materials Institute.

References and Notes

(1) Stryer, L. *Annu. Rev. Biochem.* **1978**, *47*, 819–846.
(2) Cardullo, R. A.; Agrawal, S.; Flores, C.; Zamechnik, P. C.; Wolf, D. E. *Proc. Natl. Acad. Sci. U.S.A.* **1988**, *85*, 8790–8794.
(3) Parkhurst, K. M.; Parkhurst, L. J. *J. Biomed. Opt.* **1996**, *1*, 435–441.
(4) Morreson, L. E.; Stols, L. M. *Biochemistry* **1993**, *32*, 3095–3104.

(5) Tsourkas, A.; Behlke, M. A.; Xu, Y.; Bao, G. *Anal. Chem.* **2003**, *75*, 3697–3703.
(6) Ueberfeld, J.; Walt, D. R. *Anal. Chem.* **2004**, *76*, 947–952.
(7) Wang, S.; Gaylord, B. S.; Bazan, G. C. *J. Am. Chem. Soc.* **2004**, *126*, 5446–5451.
(8) Massey, M. W.; Algar, R.; Krull, U. J. *Anal. Chim. Acta* **2006**, *568*, 181–189.
(9) Beck, P. T.; Tan, W. *Angew. Chem., Int. Ed.* **2001**, *113*, 416–419.
(10) Kong, D.-M.; Huang, Y.-P.; Zhang, X.-B.; Yang, W.-H.; Shen, H. X.; Mi, H. F. *Anal. Chim. Acta* **2003**, *491*, 135–143.
(11) McKeen, C. M.; Brown, L. J.; Nicol, J. T. G.; Mellor, J. M.; Brown, T. *Org. Biomol. Chem.* **2003**, *1*, 2267–2275.
(12) Kwok, P. Y. *Hum. Mutat.* **2002**, *19*, 315–323.
(13) Clapp, A. R.; Medinz, I. L.; Mauro, J. M.; Fisher, B. R.; Bawendi, M. G.; Mattoussi, H. **2004**, *126*, 301–310.
(14) Chen, L.; McBranch, D. W.; Wang, H. L.; Helgeson, R.; Wudl, F.; Whitten, D. G. *Proc. Natl. Acad. Sci. U.S.A.* **1999**, *96*, 12287–12292.
(15) Yang, J. S.; Swager, T. M. *J. Am. Chem. Soc.* **1998**, *120*, 11864–11873.
(16) Chen, L.; McBranch, D. W.; Wang, H.; Helgeson, R.; Wudl, F.; Whitten, D. *Proc. Natl. Acad. Sci. U.S.A.* **1999**, *96*, 12287–12292.
(17) Gaylord, B. S.; Heeger, A. J.; Bazan, G. C. *Proc. Natl. Acad. Sci. U.S.A.* **2002**, *99*, 10954–10957.
(18) Al Attar, H. A.; Norden, J.; O'Brien, S.; Monkman, A. P. *Biosens. Bioelectron.* **2008**, *23*, 1466–1472.
(19) Torimura, M.; Kurata, S.; Yamada, K.; Yokomaku, T.; Kamagata, T.; Kanagawa, T.; Kurane, R. *Anal. Sci.* **2001**, *17*, 155–161.
(20) Al Attar, H. A.; Monkman, A. P. *J. Phys. Chem. B* **2007**, *111*, 12418–12426.
(21) Liu, B.; Bazan, G. C. *J. Am. Chem. Soc.* **2006**, *128*, 1188–1196.
(22) Zheng, J.; Swager, M. *Chem. Commun.* **2004**, 2798–2799.
(23) Wong, K. F.; Bagchi, B.; Rossky, P. J. *J. Phys. Chem. A* **2004**, *108*, 5752–5763.
(24) Mallavia, R.; Montilla, F.; Pastor, I.; Velasquez, P.; Arredondo, B.; Alvarez, A. L.; Mateo, C. R. *Macromolecules* **2005**, *38*, 3185–3192.
(25) Gratton, E.; Beechem, J. *GlobalsWE*, Globals for Spectroscopy; The Laboratory for Fluorescence Dynamics: Irvine, CA, 2004.
(26) Caplin, B. E.; Rasmussen, R. P.; Bernard, P. S.; Wittwer, C. T. *Biochemica* **1999**, *1*, 5–8.
(27) *MWG Biotech Company catalog*; 2005−2006; pp 10−15.
(28) Förster, T. *Ann. Phys.* **1948**, *2*, 55–75.
(29) Lakowicz, J. R. *Principles of Fluorescence Spectroscopy*, 2nd ed.; Kluwer Academic/Plenum Publishers: New York, 1999; Ch. 4, p 129.
(30) Wong, K. F.; Bagchi, B.; Rossky, P. J. *J. Phys. Chem. A* **2004**, *108*, 5752–5763.
(31) Al Attar, H. A.; Monkman, A. P. *Adv. Funct. Mater.* **2008**, *18*, 2498–2509.
(32) http://probes.invitrogen.com/handbook/tables/2068.html.
(33) Voloshina, N. P.; Haugland, R. P.; Stewart, J. B.; Bhalgat, M. K.; Millard, P. J.; Mao, F.; Leung, W. Y.; Haugland, R. P. *J. Histochem. Cytochem.* **1999**, *47*, 1179–1188.
(34) Singer, V. Johnson, I. D. Promega, Molecular Probe, Inc. (accessed 2008), online homepage.
(35) Sun, W.-C.; Gee, K. R.; Haugland, R. P. *Bioorg. Med. Chem. Lett.* **1998**, *8*, 3107–3110.

BM801194N